*Journal of the European Ceramic Society* **15** (1995) 307–312

0955-2219/95/$9.50

# Fracture Tests for Ceramics under Mode-I, Mode-II and Mixed-Mode Loading

T. Fett, G. Gerteisen, S. Hahnenberger, G. Martin & D. Munz

Forschungszentrum Karlsruhe, Institut für Materialforschung II, and Universität Karlsruhe, Institut für Zuverlässigkeit und Schadenskunde im Maschinenbau, D 76021 Karlsruhe, Germany

(Received 26 July 1993; revised version received 2 June 1994; accepted 28 July 1994)

***Abstract***

*In the theoretical part of this paper a wide data base of stress intensity factors is presented for three types of tests appropriate for mixed-node investigations on ceramic materials. In the experimental part the test methods are applied to determine the failure behaviour of $Al_2O_3$ under mixed-mode loading. In particular, the influence of the starter crack, modelled by a narrow saw-cut and a pre-crack is illustrated.*

## 1 Introduction

Regarding ceramic material interest is increasing in the failure behaviour under mixed-mode conditions.[1-4] The aim of the investigations is:

(1) to determine the fracture toughness data $K_{Ic}$ $K_{IIc}$.
(2) to check the failure criteria by which failure under mixed-mode conditions can be predicted from the fracture toughness values $K_{Ic}$, $K_{IIc}$.

In this paper stress intensity factors will be presented for three types of tests appropriate for mixed-mode investigations. Their applications to $Al_2O_3$ will be demonstrated.

## 2 Bending Tests with Bars Containing Oblique Edge Notches

Bending specimens containing edge-cracks or narrow saw-cuts are often used in the determination of fracture toughness of ceramic materials. Whilst cracks orthogonal to the specimen surfaces are applied in $K_{Ic}$-determination, oblique edge-cracks are appropriate for mixed-mode fracture. Figure 1 illustrates the geometrical data of a specimen loaded in a four point bending test.

The stress intensity factors are given by

$$K_I = \sigma F_I \sqrt{\pi a}\,,\ K_{II} = \sigma F_{II} \sqrt{\pi a}\,;\ \sigma = \frac{3}{2}\frac{S_1 - S_2}{BW^2}P \quad (1)$$

where $B$ is the specimen thickness and $F_I$, $F_{II}$ are the geometric functions. A literature overview of these data is given in Ref. 5.

## 3 Three Point Bending with Eccentric Notch

Asymmetric bending arrangements have been studied by several authors using different methods.[6-10] In Ref. 10 the weight function method was applied. The stresses in the symmetrically supported three-point bending bar (Fig. 2) have been studied by Filon[11] who derived an analytical solution for the stress state. This solution, which take into consideration the stress magnification due to the line contacts of the rollers, is given by

$$\sigma_x = -\frac{3yPL}{2W^3} - \frac{4P}{L}\sum_{n=1}^{\infty} \frac{\sinh mW/2 - mW/2 \cosh mW/2}{mW + \sinh mW} \cos mx \cosh my$$

$$- \frac{4P}{L}\sum_{n=1}^{\infty} \frac{my \sinh mW/2}{mW + \sinh mW} \cos mx \sinh my$$

$$- \frac{4P}{L}\sum_{n=0}^{\infty} \frac{\cosh MW/2 - MW/2 \sinh MW/2}{\sinh MW - MW} \cos Mx \sinh My$$

$$- \frac{4P}{L}\sum_{n=0}^{\infty} \frac{My \cosh MW/2}{\sinh MW - MW} \cos Mx \cosh My \quad (2)$$

$$\tau = \frac{4P}{L}\sum_{n=1}^{\infty}\frac{mW/2\cosh mW/2}{mW+\sinh mW}\sin mx\sinh my$$

$$-\frac{4P}{L}\sum_{n=1}^{\infty}\frac{my\sinh mW/2}{mW+\sinh mW}\sin mx\cosh my$$

$$+\frac{4P}{L}\sum_{n=0}^{\infty}\frac{MW/2\sinh MW/2}{\sinh MW-MW}\sin Mx\cosh My$$

$$-\frac{4P}{L}\sum_{n=0}^{\infty}\frac{My\cosh MW/2}{\sinh MW-MW}\sin Mx\sinh My \quad (3)$$

with $m = 4n\pi/L$, and $M = 2(2n+1)\pi/L$

In order to determine the geometric function $F_I$ and $F_{II}$ defined by

$$K_I = \sigma_0 F_I\sqrt{\pi a}\,,\ K_{II} = \sigma_0 F_{II}\sqrt{\pi a}\,;\ \sigma_0 = \frac{3}{2}\frac{PL}{W^2B} \quad (4)$$

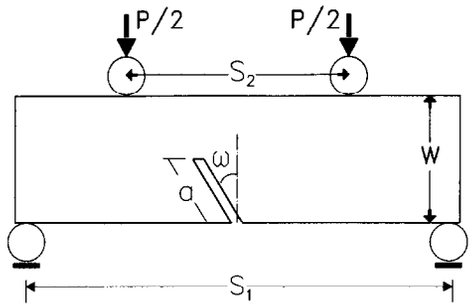


**Fig. 1.** The oblique edge-crack under four-point bending load.

**Table 1.** Geometric function for the edge-cracked plate in bending: influence of the crack length $a/W$ and the angle $\omega$ on $F_I$

| $\omega(°)$ | $a/w = 0{\cdot}1$ | 0·2 | 0·3 | 0·4 | 0·5 | 0·6 | 0·7 |
|---|---|---|---|---|---|---|---|
| 0 | 1·049 | 1·058 | 1·126 | 1·26 | 1·495 | 1·915 | 2·71 |
| 15 | 0·980 | 1·02 | 1·058 | 1·185 | 1·365 | 1·698 | 2·30 |
| 22·50 | 0·935 | 0·955 | 0·985 | 1·090 | 1·26 | 1·53 | 2·04 |
| 30 | 0·874 | 0·883 | 0·91 | 0·985 | 1·12 | 1·32 | 1·74 |
| 40 | 0·765 | 0·752 | 0·772 | 0·810 | 0·90 | 1·032 | 1·03 |
| 45 | 0·699 | 0·68 | 0·695 | 0·710 | 0·794 | 0·89 | 1·09 |
| 60 | 0·450 | 0·446 | 0·451 | 0·467 | 0·510 | 0·56 | 0·64 |
| 90 | 0 | 0 | 0 | 0 | 0 | 0 | 0 |

**Table 2.** Geometric function for the edge-cracked plate bending: influence of the crack length $a/W$ and the angle $\omega$ on $F_{II}$

| $\omega(°)$ | $a/w = 0{\cdot}1$ | 0·2 | 0·3 | 0·4 | 0·5 | 0·6 |
|---|---|---|---|---|---|---|
| 0 | 0 | 0 | 0 | 0 | 0 | 0 |
| 22·5 | 0·23 | 0·216 | 0·215 | 0·220 | 0·235 | 0·265 |
| 30 | 0·286 | 0·278 | 0·274 | 0·275 | 0·286 | 0·302 |
| 40 | 0·335 | 0·320 | 0·310 | 0·312 | 0·321 | 0·340 |
| 45 | 0·344 | 0·329 | 0·316 | 0·321 | 0·326 | 0·349 |
| 60 | 0·306 | 0·304 | 0·302 | 0·306 | 0·315 | 0·318 |
| 90 | 0 | 0 | 0 | 0 | 0 | 0 |

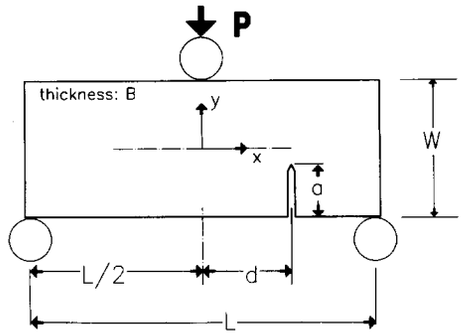


**Fig. 2.** Geometrical data of the asymmetric notched bending bar.

the mode-I and mode-II stress intensity factors were calculated by use of the mode-I and mode-II weight functions given in Ref. 10. The results are expressed by the normalized geometric functions $F'_I = F_I\,(1-a/W)^{3/2}$ and $F'_{II} = F_{II}\,(1-a/W)^{1/2}$, where

**Table 3.** Normalized geometric function for mode-I $F'_I$

| $L/W$ | $a/W$ | $2d/L = 0{\cdot}2$ | 0·4 | 0·6 | 0·7 | 0·8 | 0·9 |
|---|---|---|---|---|---|---|---|
| 2 | 0·2 | 0·6145 | 0·5032 | 0·3521 | 0·2564 | 0·1345 | −0·0011 |
| | 0·3 | 0·5240 | 0·4210 | 0·2864 | 0·2094 | 0·1274 | 0·0497 |
| | 0·4 | 0·4648 | 0·3664 | 0·2468 | 0·1837 | 0·1206 | 0·0601 |
| | 0·5 | 0·4235 | 0·3276 | 0·2194 | 0·1648 | 0·1106 | 0·0584 |
| 3 | 0·2 | 0·6179 | 0·4755 | 0·3252 | 0·2496 | 0·1604 | 0·0344 |
| | 0·3 | 0·5315 | 0·4067 | 0·2745 | 0·2070 | 0·1331 | 0·0533 |
| | 0·4 | 0·4720 | 0·3581 | 0·2398 | 0·1801 | 0·1187 | 0·0571 |
| | 0·5 | 0·4280 | 0·3220 | 0·2148 | 0·1615 | 0·1079 | 0·0547 |
| 4 | 0·2 | 0·6187 | 0·4625 | 0·3111 | 0·2399 | 0·1651 | 0·0607 |
| | 0·3 | 0·5330 | 0·3989 | 0·2673 | 0·2034 | 0·1364 | 0·0597 |
| | 0·4 | 0·4729 | 0·3536 | 0·2362 | 0·1785 | 0·1194 | 0·0583 |
| | 0·5 | 0·4278 | 0·3196 | 0·2132 | 0·1605 | 0·1075 | 0·0545 |
| 8 | 0·2 | 0·6101 | 0·4553 | 0·3035 | 0·2282 | 0·1551 | 0·0825 |
| | 0·3 | 0·5279 | 0·3945 | 0·2630 | 0·1976 | 0·1333 | 0·0682 |
| | 0·4 | 0·4692 | 0·3511 | 0·2341 | 0·1757 | 0·1180 | 0·0597 |
| | 0·5 | 0·4250 | 0·3184 | 0·2123 | 0·1593 | 0·1065 | 0·0537 |

**Table 4.** Normalized geometric function for mode-II

| $L/W$ | $a/W$ | $2d/L = 0{\cdot}2$ | 0·4 | 0·6 | 0·7 | 0·8 | 0·9 |
|---|---|---|---|---|---|---|---|
| 2 | 0·2 | 0·0557 | 0·0868 | 0·1069 | 0·1359 | 0·2146 | 0·3893 |
| | 0·3 | 0·0743 | 0·1167 | 0·1453 | 0·1750 | 0·2315 | 0·3093 |
| | 0·4 | 0·0899 | 0·1378 | 0·1649 | 0·1858 | 0·2172 | 0·2522 |
| | 0·5 | 0·1041 | 0·1513 | 0·1709 | 0·1825 | 0·1979 | 0·2116 |
| 3 | 0·2 | 0·0553 | 0·0696 | 0·0638 | 0·0649 | 0·0871 | 0·1912 |
| | 0·3 | 0·0712 | 0·0895 | 0·0856 | 0·0895 | 0·1131 | 0·1779 |
| | 0·4 | 0·0827 | 0·1018 | 0·0995 | 0·1036 | 0·1206 | 0·1550 |
| | 0·5 | 0·0915 | 0·1081 | 0·1063 | 0·1091 | 0·1189 | 0·1358 |
| 4 | 0·2 | 0·0497 | 0·0543 | 0·0481 | 0·0454 | 0·0499 | 0·1049 |
| | 0·3 | 0·0633 | 0·0693 | 0·0632 | 0·0616 | 0·0692 | 0·1131 |
| | 0·4 | 0·0722 | 0·0781 | 0·0730 | 0·0723 | 0·0793 | 0·1062 |
| | 0·5 | 0·0777 | 0·0820 | 0·0783 | 0·0779 | 0·0827 | 0·0971 |
| 8 | 0·2 | 0·0276 | 0·0259 | 0·0258 | 0·0253 | 0·0236 | 0·0249 |
| | 0·3 | 0·0352 | 0·0333 | 0·0332 | 0·0328 | 0·0311 | 0·0345 |
| | 0·4 | 0·0395 | 0·0378 | 0·0377 | 0·0373 | 0·0361 | 0·0396 |
| | 0·5 | 0·0413 | 0·0400 | 0·0400 | 0·0397 | 0·0388 | 0·0413 |

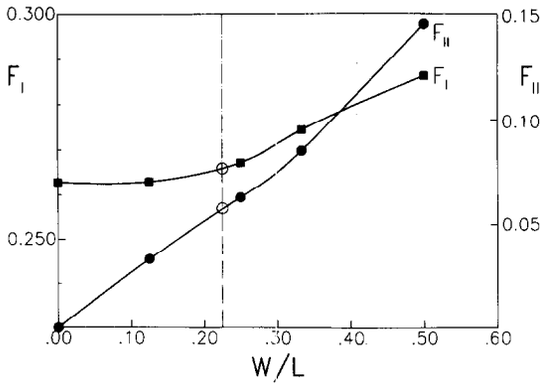


**Fig. 3.** Interpolations for the two geometric functions $F_I$ and $F_{II}$ (three-point bending with eccentric crack).

$F_I$, $F_{II}$ are defined by eqn (4). Data for $F'_I$ are entered in Table 3 and Table 4 contains values of $F'_{II}$.

Tables 3 and 4 allow geometric functions for a wide range of $L/W$ ratios to be interpolated. Since additionally the values for $L/W \to \infty$ are known, namely

$$F_I\Big|_{L/W=\infty} = \left(1-2\frac{d}{L}\right) F_I\Big|_{L/W=\infty,\, d/L=0} \tag{5a}$$

$$F_{II}\Big|_{L/W=\infty} = 0 \tag{5b}$$

all $L/W$-values in the range $2 \le L/W < \infty$ can be evaluated. For the geometric function $F_I$ at $d/L = 0$ the solution of Nisitani and Mori[12] may be applied.

$$F_I = 1{\cdot}122 - 1{\cdot}121\alpha + 3{\cdot}74\alpha^2 + 3{\cdot}873\alpha^3 - 19{\cdot}05\alpha^4 + 22{\cdot}55\alpha^5 \tag{5c}$$

For practical use interpolation of $W/L$ instead of $L/W$ is recommended as illustrated im Fig. 3 for the geometrical data ($L$ = 20 mm, $W$ = 4·5 mm) used in the experimental part.

## 4 The Asymmetric Four-point Bending Test

For the determination of the fracture toughness $K_{IIc}$ with edge-notched (or pre-cracked) beams asymmetric bending arrangements (Fig. 4) are recommended which show a negligible mode-I contribution. Stress intensity factors have been determined for special geometrics by FE-calculations

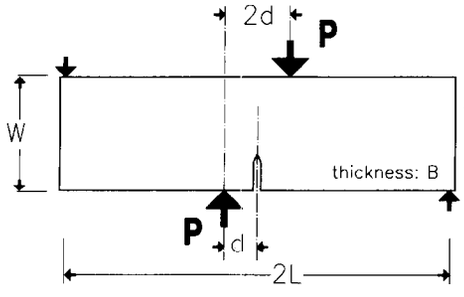


**Fig. 4.** Geometrical data of the asymmetrically loaded notched bending bar.

**Table 5.** Geometric function for mode II

| $a/W$ | $d/W = 0{\cdot}25$ | 0·300 | 0·375 | 0·500 | 0·625 |
|---|---|---|---|---|---|
| 0·1 | 0·3746 | 0·3428 | 0·3318 | 0·3450 | 0·3599 |
| 0·2 | 0·7881 | 0·7180 | 0·6719 | 0·6633 | 0·6741 |
| 0·3 | 1·0374 | 0·9933 | 0·9560 | 0·9399 | 0·9431 |
| 0·4 | 1·1858 | 1·1819 | 1·1753 | 1·1702 | 1·1695 |
| 0·5 | 1·3120 | 1·3380 | 1·3579 | 1·3661 | 1·3641 |
| 0·6 | 1·4674 | 1·5079 | 1·5387 | 1·5507 | 1·5472 |
| 0·7 | 1·6948 | 1·7318 | 1·7553 | 1·7600 | 1·7547 |
| 0·8 | 2·053 | 2·0687 | 2·073 | 2·0684 | 2·0635 |
| 0·9 | 2·7563 | 2·7545 | 2·7505 | 2·7467 | 2·7452 |

**Table 6.** Geometric function for mode I

| $a/W$ | $d/W = 0{\cdot}25$ | 0·300 | 0·375 | 0·500 | 0·625 |
|---|---|---|---|---|---|
| 0·1 | 0·2615 | 0·3695 | 0·4241 | 0·3841 | 0·2918 |
| 0·2 | –0·0038 | 0·1129 | 0·2110 | 0·2448 | 0·2060 |
| 0·3 | –0·0307 | 0·0447 | 0·1184 | 0·1580 | 0·1410 |
| 0·4 | 0·0024 | 0·0483 | 0·0904 | 0·1098 | 0·09534 |
| 0·5 | 0·0407 | 0·0672 | 0·0842 | 0·0806 | 0·06268 |
| 0·6 | 0·0716 | 0·0808 | 0·0771 | 0·0566 | 0·03706 |
| 0·7 | 0·0855 | 0·0769 | 0·0581 | 0·03198 | 0·0164 |
| 0·8 | 0·0641 | 0·0460 | 0·0271 | 0·0106 | 0·00359 |
| 0·9 | –0·0048 | –0·0002 | 0·0077 | 0·01406 | 0·0138 |

and energy considerations[9–14] and for a wide range of geometries by the weight function method.[15]

The stresses in this loading case were also computed by Filon[11] with formulae similar to eqns (2) and (3). The geometric functions $F_I$ and $F_{II}$ defined by

$$K_I = \frac{P}{WB}\left(1-\frac{d}{L}\right)\sqrt{\pi a}F_I,\; K_{II} = \frac{P}{WB}\left(1-\frac{d}{L}\right)\sqrt{\pi a}F_{II} \tag{6}$$

are given in Table 5 and 6.[15]

As can be seen from Table 6, the geometric function $F_{II}$ is approximately independent of the value of $d/W$ in the range $0{\cdot}375 \le d/W \le 0{\cdot}625$. An analytical approximation can be given by

$$F_{II} = 3{\cdot}9204\alpha - 5{\cdot}1295\alpha^2 + 14{\cdot}4566\alpha^3 - 26{\cdot}2916\alpha^4 + 17{\cdot}073\alpha^5,\; \alpha = a/W \tag{7}$$

## 5 Experiments

### 5.1 Failure diagram for edge-notched specimens

Mixed-mode fracture tests were performed with bending bars having the dimensions $B$ = 3·5 mm, $W$ = 4·5 mm and length >43 mm, made of two $Al_2O_3$–ceramics (material I: $Al_2O_3$+ 3% $SiO_2$, V37; material II: 99.1% $Al_2O_3$, B40; both materials from Feldmühle AG, Plochingen). The specimens were edge-notched with saw-cuts of 50 $\mu$m width. Several specimens were provided with oblique notches, angles $\omega$ = 0°, 22·5°, 30° and 40° and relative notch lengths in the range of $0{\cdot}1 < a/W < 0{\cdot}4$. In Fig. 5 the mode-I stress intensity factors at failure are plotted versus the mode-II stress intensity factors for material

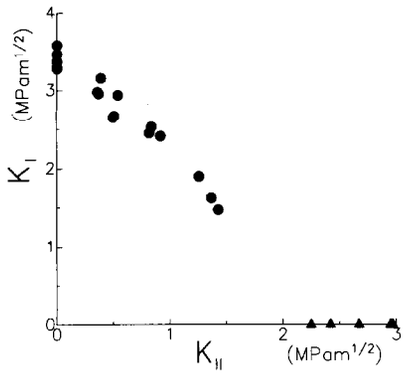


**Fig. 5.** $K_I$ vs $K_{II}$ at failure for $Al_2O_3$ (material I); circles: eccentric three-point bending test, triangles: asymmetric four-point bending test.

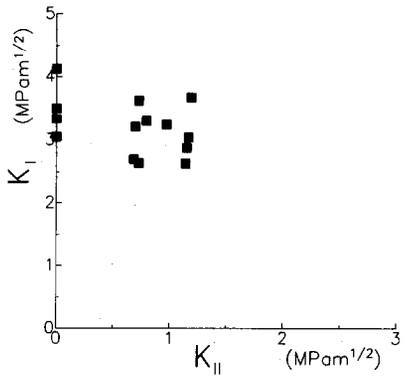


**Fig. 6.** $K_I$ vs $K_{II}$ at failure for $Al_2O_3$ (material II) measured with oblique edge notched specimens.

I. The circles represent fracture tests carried out in three-point bending arrangements with eccentric notch (Fig. 2), $a/W = 0{\cdot}35$–$0{\cdot}5$, $L = 20$ mm; the triangles were determined in the asymmetric four-point bending test with $a/W \simeq 0{\cdot}45$–$0{\cdot}5$, $L = 20$ mm, $d = 5$ mm. Figure 6 shows results obtained for material II. The data are obtained in tests with oblique notches. The differences in the $K_I$–$K_{II}$ dependencies shown in Figs 5 and 6 seem to be caused more by the specific material properties than by the different types of measurement.

### 5.2 Mode-I and mode-II fracture toughness

Fracture toughness measurements were carried out in three and four-point bending tests with different starter cracks. Small saw-cuts were introduced as well as sharp pre-cracks produced with the bridging method. Some of the precracked specimens were annealed in order to remove residual stresses caused by the bridging procedure, and some pre-cracked specimens were renotched so that $\simeq$ 80–90% of the original crack was removed. The results are shown in Tables 7 and 8.

The numbers in the column heads of the tables denote the test procedure.

1 — saw-cut ($a/W = 0{\cdot}33$), four-point bending (inner roller span 20 mm, outer roller span 40 mm);

**Table 7.** $K_{Ic}$, $Al_2O_3$: (material I)

| 1 | 2 | 3 | 4 | 5 |
|---|---|---|---|---|
| 3·28 | 3·08 | 3·02 | 3·44 | 2·93 |
| 3·59 | 2·69 | 3·31 | 3·27 | 3·25 |
| 3·47 | 2·84 | 3·50 | 3·28 | 3·32 |
| 3·37 | 2·80 | 3·58 | 3·23 | 3·14 |
| 3·30 | 2·98 | 3·59 | 3·36 | 3·14 |
| $K_{Ic} = 3{\cdot}40$ | 2·88 | 3·40 | 3·32 | 3·16 |

**Table 8.** $K_{IIc}$, $Al_2O_3$: (material I)

| 6 | 7 | 8 |
|---|---|---|
| 2·42 | 4·16 | 4·56 |
| 2·67 | 5·15 | 5·01 |
| 2·97 | 4·90 | |
| 2·25 | 5·19 | |
| 2·95 | | |
| $K_{Ic} = 2{\cdot}65$ | 4·85 | 4·8 |

2 — pre-cracked ($a/W \simeq 0{\cdot}45$), four-point bending (inner roller span 20 mm, outer roller span 40 mm);

3 — pre-cracked and annealed ($a/W \simeq 0{\cdot}45$), four-point bending (inner roller span 20 mm, outer roller span 40 mm);

4 — saw-cut ($a/W \simeq 0{\cdot}33$), three-point bending (roller span 20 mm);

5 — pre-cracked ($a/W \simeq 0{\cdot}4$–$0{\cdot}35$), three-point bending (roller span 20 mm),

6 — saw-cut ($a/W = 0{\cdot}47$), asymmetric four-point bending;

7 — pre-cracked ($a/W \simeq 0{\cdot}45$–$0{\cdot}50$), asymmetric four-point bending;

8 — pre-cracked and re-notched ($a/W \simeq 0{\cdot}47$), asymmetric four-point bending.

### 5.3 Influence of the starter crack on the failure diagram

Mixed-mode strength tests were carried out in eccentric three-point bending with the different crack types. Figure 7 shows the results for $Al_2O_3$ (material I) for specimens with saw-cuts, pre-cracks and re-notched cracks. In Fig. 7 also mode-I fracture toughness data are introduced (small solid circles) which were obtained with pre-cracked specimens annealed for 5 h at 900°C in the vacuum (third column of Table 7).

## 6 Discussion and Conclusions

### 6.1 Fracture toughness of $Al_2O_3$

- The mode-I fracture toughness $K_{Ic}$ of $Al_2O_3$ has been found to be

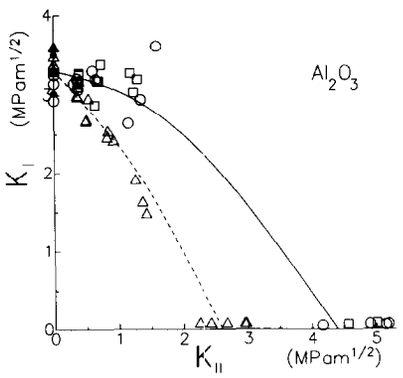


**Fig. 7.** $K_I$ vs $K_{II}$ at failure for $Al_2O_3$ measured in eccentric three-point bending tests and asymmetric four-point bending tests. Triangles: specimens with saw-cut, circles: pre-cracked with bridging method, squares: pre-cracked and re-notched specimens, solid circles: pre-cracked and annealed.

3·40 ± 0·13 MPa $\sqrt{m}$ for the edge-notched specimens in four-point bending;
3·32 ± 0·08 MPa $\sqrt{m}$ for the edge-notched specimens in three-point bending;
3·40 ± 0·24 MPa $\sqrt{m}$ for the specimens with an edge-precrack which has been annealed;
3·16 ± 0·14 MPa $\sqrt{m}$ for the specimens with an edge-precrack (without annealing) in three-point bending; and
2·88 ± 0·15 MPa $\sqrt{m}$ for the same specimens in four-point bending.

It is obvious that within the scatter ranges the edge-notched specimens show the same results as the pre-cracked and subsequently annealed specimens.

The precracked specimens which were not annealed show a reduced fracture toughness. One can conclude that the fracture toughness data obtained with pre-cracked specimens are reduced due to internal stresses caused by a misfit between the two crack surfaces. This effect overcompensates an expected *R*-curve effect which would yield an increase in $K_{Ic}$ for the pre-cracked specimens.

- Under mode-II loading the pre-cracked specimens showed — in contrast to the mode-I results — significantly higher fracture toughness than the notched specimens:
  2·65 ± 0·3 MPa $\sqrt{m}$ for notched specimens;
  4·85 ± 0·3 MPa $\sqrt{m}$ for pre-cracked specimens;
  ≃4·8 MPa $\sqrt{m}$ for pre-cracked and then partially re-notched specimens.

  These results may be explained by crack surface interactions. Under mode-II loading the rough surface of the pre-crack can carry a part of the externally applied load and, therefore, the actual crack tip stress intensity factor is reduced, i.e. a crack-shielding effect occurs. Consequently, the applied load has to be increased to reach the critical crack tip stress intensity factor that is necessary for the onset of stable crack propagation followed by catastrophic failure.

From the fact that in the case of partially re-notched specimens (≃80–90% of the pre-crack were re-notched) the $K_{IIc}$ is nearly unaffected by the re-notch procedure we conclude that the main part of mode-II crack shielding effect occurs directly in the neighbourhood of the crack tip.

- The ratio of the mode-II and mode-I fracture toughness results for the notched specimens is $K_{IIc}/K_{Ic} = 0·78$.

### 6.2 Conclusion

Several types of starter cracks have been used in mixed-mode fracture tests, namely

- edge-notched specimens (saw-cut of 50 $\mu$m width);
- pre-cracked specimens (bridge method);
- pre-cracked and subsequently annealed specimens;
- pre-cracked and subsequently re-notched specimens.

If a rising crack-growth resistance curve exists, the tests with specimens with a saw-cut lead to $K_{Ic}$-values at the onset of crack extension provided that the notch width is small enough. The results for the $Al_2O_3$ investigated were:

$$K_{Ic} = 3·4 \text{ MPa } \sqrt{m}\,, \quad K_{IIc} = 2·65 \text{ MPa } \sqrt{m}\,, \quad K_{IIc}/K_{Ic} = 0·78$$

As a general result of the measurements presented it is recommended to prefer edge-notched specimens for mode-I and mode-II fracture toughness measurements.

## References

1. Petrovic, J. J., Mixed-mode fracture of ceramics. In *Fracture Mechanics of Ceramics*. Plenum Press, New York, Vol. 8, 1986, pp. 127–35.
2. Petrovic, J. J., Mixed-mode fracture of hot-pressed $Si_3N_4$. *J. Am. Ceram. Soc.*, **68** (1985) 348–55.
3. Shetty, D. K., Rosenfield, A. R. & Duckworth, W. H., Mixed-mode fracture of ceramics from surface flaws in diametral-compression. *J. Am. Ceram. Soc.*, **69** (1986) 437–43.
4. Shetty, D. K., Rosenfield, A. R. & Duckworth, W. H., Mixed-mode fracture in biaxial stress state: application of the diametral-compression (Brazilian disk) test. *Engng Fract. Mech.*, **26** (1987) 825–40.
5. Fett, T., Mixed-mode stress intensity factors for the oblique edge-crack in rectangular specimens. *Int. J. Fract.*, **61** (1993) R3–R10.
6. Jen, W. K., Lin, H. C. & Hua, K., Calculation of stress intensity factors for combined mode bend specimens. In *Fracture*, ed. D. M. R. Taplin. Pergamon Press, Oxford, 1977, Vol. 4., pp. 123–33.
7. Gao, H., Chang, S., Combined mode I–mode II fracture. *Acta Metall. Sinica*, **12** (1981) 1–15 (in Chinese).
8. Maccango, T. M. & Knott, J. F., Brittle fracture under mixed mode I/mode II loading. In *Fracture Control of Engineering Structures, European Conference on Fracture 6* ed. H. C. van Elst and A. Bakker. Engng Mater. Adv. Services, Warley, 1986.
9. Suresh, S., Shih, C. F., Morrone, A. & O'Dowd, N. P., Mixed-mode fracture toughness of ceramic materials. *J. Am. Ceram. Soc.*, **73** (1990) 1257–67.

10. Fett, T., Mixed-mode stress intensity factors for three-point bending bars. *Int. J. Fract.*, **48** (1991) R67–R74.
11. Filon, L. N. G., On an approximate solution for the bending of a beam of rectangular cross-section under any system of load, with special reference to points of concentrated or discontinuous loading. *Phil. Trans., A*, **201** (1903) 63–155.
12. Nistani, H. & Mori, K., Tech Reports of the Kyushu Univ. Vol. 58 (1985), pp. 751–5.
13. Otsuka, A., Tohgo, T., Kiba, T. & Yamada, S., Mode-II fatigue crack growth characteristics and mechanism in aluminium alloy 7N01-T4 weldments under mode-II loading. *Advances in Fracture Research, Proc. ICF 6*, 3, Pergamon, Oxford, 1984, pp. 1671–8.
14. Hem, M.Y., Cao, H. C. & Evans, A. G., Mixed-mode fracture: The four-point shear specimen. *Acta Metall. Mater.*, **38** (1990) 839–46.
15. Fett, T., Stress intensity factors for edge crack subjected to mixed mode four-point bending. *Theor. Appl. Fract. Mech.*, **15** (1991) 99–104.